

# Photo-spin-voltaic effect

David Ellsworth<sup>1†</sup>, Lei Lu<sup>1†</sup>, Jin Lan<sup>2,3</sup>, Houchen Chang<sup>1</sup>, Peng Li<sup>1</sup>, Zhe Wang<sup>3</sup>, Jun Hu<sup>2</sup>, Bryan Johnson<sup>1</sup>, Yuqi Bian<sup>1</sup>, Jiang Xiao<sup>3,4</sup>, Ruqian Wu<sup>2,3\*</sup> and Mingzhong Wu<sup>1\*</sup>

The photo-voltaic effect typically occurs in semiconductors and involves photon-driven excitation of electrons from a valence band to a conduction band. In a region such as a p-n junction that has a built-in electric field, the excited electrons and holes diffuse in opposite directions, resulting in an electric voltage. This letter reports that a spin voltage can be created by photons in a non-magnetic metal that is in close proximity to a magnetic insulator: a photo-spin-voltaic effect. The experiments use platinum/magnetic insulator bilayer structures. On exposure to light, there occurs photon-driven, spin-dependent excitation of electrons in several platinum atomic layers near the platinum/magnetic insulator interface. The excited electrons and holes diffuse in different manners, and this gives rise to an effective spin voltage at the interface and a corresponding pure spin current that flows across the platinum.

Conventional microelectronics relies on the charges of electrons for information transfer and processing. With ever-growing capacities and functionalities, however, charge-current-associated power consumption in electronic devices has become an increasingly severe issue. In addition to charges, electrons also carry spins. It is possible to drive electrons with different spins to flow in opposite directions, producing a spin current rather than a charge current. Such spin currents can potentially be used to develop a new generation of electronics that consumes significantly lower energy.

The generation of pure spin currents in a rapid and controllable manner represents a challenging research subject. At the present time, pure spin currents can be generated by means of spin pumping and the spin Seebeck effect (SSE). Spin pumping involves the use of microwaves to drive the precession of magnetic moments in a ferromagnet and the transfer of spins from precessional moments to an adjacent normal metal<sup>1–3</sup>. For the SSE, a temperature gradient across a ferromagnetic film induces a spin voltage in the film which can inject a spin current into an adjacent normal metal<sup>4–10</sup>. Although spin pumping and the SSE offer two means for spin current generation, it is challenging to realize well-localized microwave fields or temperature gradients at nanometre scales in a rapid fashion. An alternative way to produce pure spin currents is to use the spin Hall effect, in which spin-orbit coupling converts a longitudinal charge current to a transverse spin current<sup>11–14</sup>. This approach, however, requires charge currents, and hence involves unwanted power consumption.

This letter reports on the discovery of a photo-spin-voltaic (PSV) effect that offers a new means for the generation of pure spin currents. A schematic of the effect is shown in Fig. 1. The experiments used normal metal/magnetic insulator (MI) heterostructures where the normal metal was a Pt layer, several nanometres in thickness, and the MI was a film of Y<sub>3</sub>Fe<sub>5</sub>O<sub>12</sub> (YIG)<sup>15</sup>, Ga-doped YIG, or BaFe<sub>12</sub>O<sub>19</sub> (BaM)<sup>16</sup> with a thickness in the 10–10<sup>5</sup> nm range. When light illuminates the Pt film, photons with appropriate energy excite electrons in the occupied bands to the unoccupied bands. For the Pt atomic layers in close proximity to the MI, the efficiency of

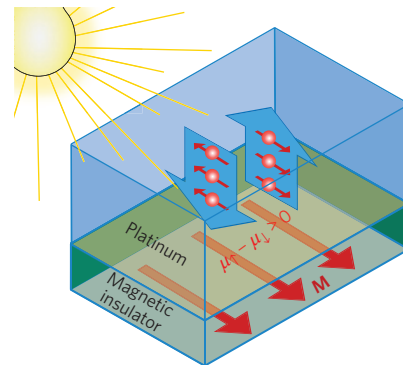
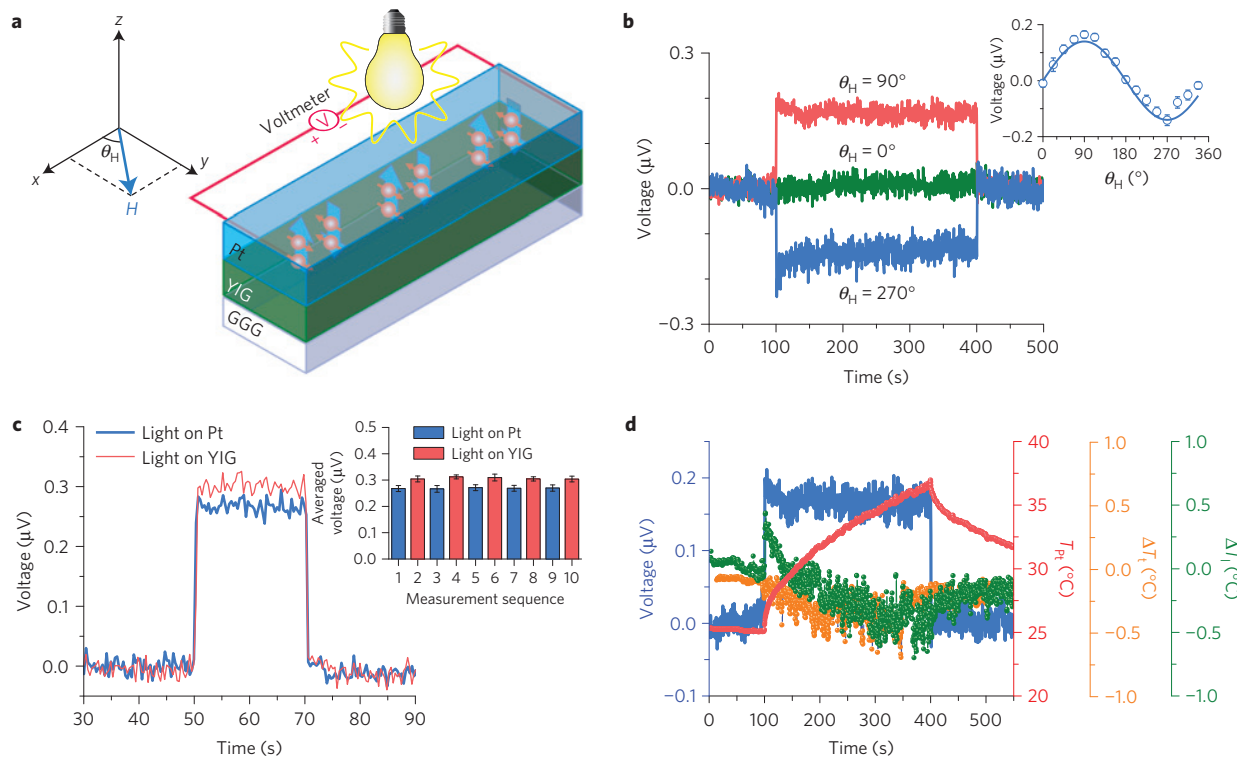


**Figure 1 | Photo-spin-voltaic effect in a platinum (Pt)/magnetic insulator (MI) bi-layered structure.** The MI has in-plane magnetization (**M**). When the structure is exposed to light, a spin voltage ( $\mu_{\uparrow} - \mu_{\downarrow}$ ) arises in Pt atomic layers in close proximity to the MI. This spin voltage drives spin-up and spin-down electrons to move in opposite directions, resulting in a pure spin current across the Pt thickness.

the photon-driven electron excitation is different for electrons in different spin channels. This efficiency difference, together with the difference in the diffusion of the excited electrons and holes, gives rise to a spin voltage near the interface, and a corresponding pure spin current across the Pt thickness. Such spin currents can produce a measurable electric voltage in the Pt film by means of the inverse spin Hall effect (ISHE)<sup>12,17</sup>. This new phenomenon is analogous to the photo-voltaic effect in semiconductors<sup>18</sup>, but engages spin-dependent photon-driven electron excitation.

Figure 2a shows a schematic of the experimental set-up, where the core component is a Pt(2.5 nm)/YIG(4.9  $\mu$ m) structure grown on a Gd<sub>3</sub>Ga<sub>5</sub>O<sub>12</sub> (GGG) substrate. An in-plane magnetic field **H** is applied to magnetize the YIG film to saturation. A halogen light bulb was used to illuminate the Pt/YIG structure from either the top (as shown) or the bottom. A nanovoltmeter was used to measure ISHE voltages across the Pt length.

<sup>1</sup>Department of Physics, Colorado State University, Fort Collins, Colorado 80523, USA. <sup>2</sup>Department of Physics and Astronomy, University of California, Irvine, California 92697, USA. <sup>3</sup>State Key Laboratory of Surface Physics and Key Laboratory for Computational Physical Sciences and Department of Physics, Fudan University, Shanghai 200433, China. <sup>4</sup>Collaborative Innovation Center of Advanced Microstructures, Fudan University, Shanghai 200433, China. <sup>†</sup>These authors contributed equally to this work. \*e-mail: wur@uci.edu; mwu@colostate.edu



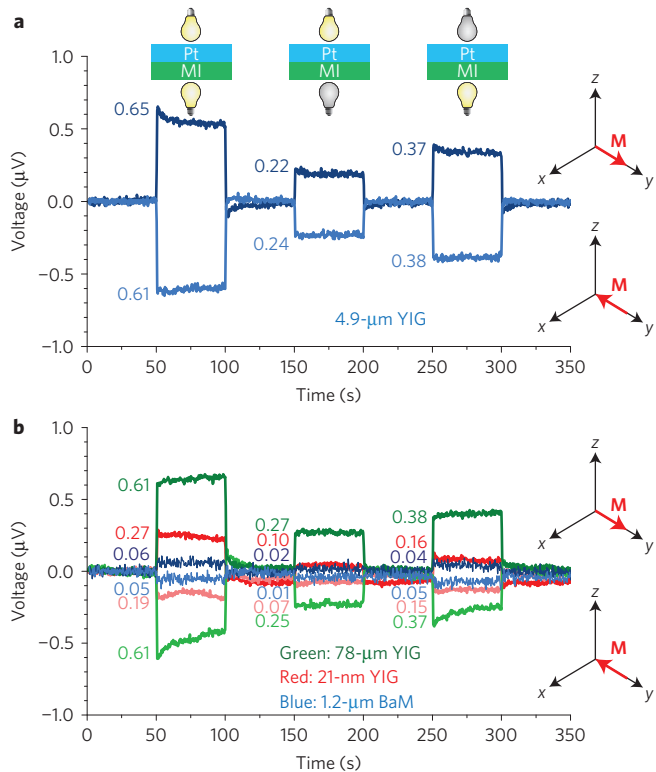
**Figure 2 | Main features of the PSV effect.** **a**, Experimental configuration to demonstrate the PSV effect. **b**, Voltage signals measured for different field angles ( $\theta_H$ ) in response to light that was first turned on at 100 s and then turned off at 400 s. The inset shows the voltage as a function of  $\theta_H$ . The circles show the voltage average over the entire period of light illumination; the error bars represent the standard deviation; the curve shows a sine function fit. **c**, Voltage signals for different directions of light illumination in response to a light signal turned on at 50 s and off at 70 s. The inset shows the voltage values for ten measurements, which are averages over the time period of 55–65 s; error bars are the standard deviation. **d**, Voltage and temperature profiles obtained under the same condition as the data shown by the red curve in **b**. All the data were obtained with a 3.5-mm-long, 1.5-mm-wide Pt(2.5 nm)/YIG(4.9  $\mu$ m)/GGG(0.5 mm) sample, a magnetic field of  $H=1,090$  Oe, and a 100-W halogen light bulb placed 29 cm away from the sample. The data in **b** and **d** were measured with an electrode separation of 2.5 mm, whereas the data in **c** were measured with a separation of 3.0 mm. For the data in **c** and **d**, the field angle  $\theta_H$  is 90°.

Figure 2b shows the voltage signals measured in response to light illuminating the Pt side of the structure. The three signals are for different field angles ( $\theta_H$ , as marked in Fig. 2a). Figure 2c compares the responses to light incident on different sides of the sample. One can see three main results from the data in Fig. 2b,c. First, the light illumination gives rise to a notable voltage signal, demonstrating the PSV effect. Second, the voltage versus  $\theta_H$  response can be fitted well by a sine curve, with the voltage flipping its sign when  $H$  is reversed, showing the magnetic nature of the PSV effect. Third, reversal of the direction of light illumination does not result in a change in the sign of the voltage, indicating that the PSV effect is unrelated to possible temperature gradients across the structure thickness.

Figure 2d presents measurements of the voltage and three temperatures, which further confirm the irrelevance of the temperature gradient. The blue curve shows the voltage. The red, orange, and green symbols show the temperature of the Pt surface ( $T_{Pt}$ ), the temperature difference across the entire structure thickness ( $\Delta T_t$ ), and the temperature difference along the  $x$  axis between the two electrodes for the voltage measurements ( $\Delta T_l$ ), respectively. It is obvious that the temperatures respond to the ‘on’ and ‘off’ operations of the light in a manner much slower than that of the voltage.  $\Delta T_t$  even changes its sign during the period of light illumination. Furthermore,  $\Delta T_t$  and  $\Delta T_l$  are both very small, with their absolute values less than 0.5 °C. If one takes into account the GGG substrate thickness and assumes a linear temperature distribution across the structure thickness, the temperature difference across the YIG film thickness would be less than 0.005 °C. These results together clearly confirm that

the observed voltage signals cannot be attributed to any effects associated with a temperature gradient, including the Seebeck effect<sup>19</sup>, the SSE<sup>4–10</sup>, the Nernst effect<sup>20</sup>, the anomalous Nernst effect<sup>21,22</sup>, and the planar Nernst effect<sup>21,23–25</sup>. Note that when  $\Delta T_t$  ( $\Delta T_l$ ) is large and the SSE overwhelms the PSV effect, the voltage signal changes with time in the exactly same manner as  $\Delta T_t$  ( $\Delta T_l$ ), as shown in Supplementary Fig. 4.

The above-described PSV effect was further examined through control measurements. Figure 3 shows data obtained with different light/field configurations using four different samples. Figure 3a shows the data for the same sample as described in Fig. 2. The data were obtained for three light configurations and two different magnetization (M) orientations. The numbers beside the voltage profiles indicate the voltage levels. Three important results are evident from Fig. 3a. First, for a given M orientation, the voltage signal is the strongest when the two bulbs are used to illuminate both the sides of the sample; and there is no change in the voltage sign when one switches between the light-on-Pt and light-on-MI configurations. These results further verify that the observed effect is not due to any effects associated with a temperature gradient. If the effect is associated with temperature gradients, one would expect that, for the three light configurations in Fig. 3a, the leftmost one should have the smallest temperature gradient across the MI thickness, and should therefore yield the weakest voltage signal. Second, the data also show that the voltage obtained with two bulbs illuminating both sample sides is approximately equal to the sum of the voltages for the light-on-MI and light-on-Pt configurations. This result indicates that it is the light intensity, not the illumination



**Figure 3 | Measurements for different illumination/magnetization configurations.** The data show PSV voltages in response to three different light illumination configurations (see small diagrams on the top) for two different magnetization (**M**) orientations (see diagrams on the right) for four different samples. **a**, Results for the same sample as that described in Fig. 2. **b**, Results for three further samples. '78-μm YIG' denotes a 18-mm-long, 1.65-mm-wide Pt(2.6 nm)/Ga-doped-YIG(78 μm)/GGG (0.4 mm) sample, '21-nm YIG' denotes a 4.1-mm-long, 2.3-mm-wide Pt(2.5 nm)/YIG(21 nm)/GGG(0.5 mm) sample, and '1.2-μm BaM' denotes a 4.1-mm-long, 2.5-mm-wide Pt(2.5 nm)/BaM(1.2 μm)/sapphire(0.6 mm) sample. All the data were obtained with 100-W halogen light bulbs. The light-to-sample distances were 20 cm, and the electrode separation was about 3.8 mm.

direction, which is important for the PSV effect. Third, reversing **M** results in a flip in the sign of the voltage, but produces only trivial changes in the voltage magnitude, confirming the magnetic nature of the PSV effect shown in Fig. 2b.

Figure 3b presents the data measured with three different samples, where the MI layers are a 78-μm-thick opaque Ga-doped YIG film, a 21-nm-thick transparent YIG film, and a 1.2-μm-thick brown-colour BaM film. The data are presented in the same format as in Fig. 3a. One can see that the data in Fig. 3b evidently confirm all the results shown in Fig. 3a. Moreover, they also suggest it is most likely that visible light does not play a dominant role in the PSV effect. If visible light were to be involved then one would expect that the samples consisting of non-transparent MI films should yield much weaker signals for the light-on-MI configuration than for the light-on-Pt configuration.

The data in Fig. 3 indicate a very important result: in spite of very different magnetic films, the four samples yielded voltage signals that differ by no more than one order of magnitude. This result has two implications: the signals are not due to the SSE, which depends strongly on the MI thickness<sup>26</sup>; and the effect is not associated with magnon excitations in the MI, but is probably related to excitations in the Pt. If the MI is responsible for the PSV effect, one would expect that the voltage levels of the signals from the three YIG samples should be significantly different. In addition, the data also indicate

that, independent of the thickness and transparency of the MI, the light-on-MI configuration gives stronger signals than the light-on-Pt configuration, consistent with the data shown in Fig. 2c.

The above results indicate that it is very likely that the PSV effect relies on excitations in the Pt and visible light does not make the major contribution. These indications were further clarified by measurements using different light sources and optical filters. Figure 4 shows representative data. Figure 4a presents the optical transmission values of four samples grown on GGG substrates, as well as the transmission of a bare GGG substrate. Although not shown, the transmission values in each case remained the same when the samples were flipped over. In comparison with the bare GGG, the two YIG samples show much lower transmission values in the 350–450 nm range. This is consistent with the fact that YIG films have a bandgap of about 2.8 eV (ref. 27). The comparison between the data of the YIG and Pt/YIG samples clearly shows that the growth of a Pt capping layer results in a notable reduction in the transmission of the sample. This result, together with the fact that the Pt layers are significantly thinner than the YIG films, indicates strong light–Pt interactions, thereby indirectly supporting the above-discussed result that the PSV effect is related to the excitations in the Pt.

Figure 4b presents the voltages obtained when optical filters were inserted between the light bulb and the sample. The figure shows the voltage data for 12 filter combinations, all normalized to the voltage measured with no filters. The figure also includes results which were calculated by using a multiplication rule and the data measured with a single filter inserted. As explained in the Supplementary Information, the main argument in the multiplication rule is that the agreement of the measured voltages with the calculated values would indicate that the PSV effect occurs only in a narrow light wavelength ( $\lambda$ ) range, whereas the disagreement would suggest that light over a wide wavelength range contributes to the PSV effect. One can see from Fig. 4b that the experimental voltages agree well with the calculated values for all 12 configurations, which evidently indicates that only a relatively narrow wavelength range, rather than a broad spectrum, is responsible for the PSV effect.

To further identify the critical wavelength, several measurements were carried out as described below. First, measurements were performed that used a 40-W white LED lamp with the spectrum shown in Fig. 4c, instead of the halogen bulb. The measurements, however, yielded very weak signals. This result confirms the above conclusion that the visible light does not make a major contribution. Second, measurements that used a filter with the transmission shown in Fig. 4d gave a very strong signal (92.2% of the signal obtained with no filters). This result further confirms that light with  $\lambda < 700$  nm does not play a major role. Third, as shown in Fig. 4e, measurements using a 800-nm short-pass filter and a 900-nm long-pass filter indicate that light in the range  $700 \text{ nm} < \lambda < 1,000 \text{ nm}$  also makes a very small contribution to the PSV effect. Note that the voltage (0.18 μV) measured with both the 800S and 900L filters used is very close to the value (0.17 μV) calculated using the multiplication rule, which firmly suggests that light in the range  $700 \text{ nm} < \lambda < 1,000 \text{ nm}$  is not responsible for the PSV effect. Finally, as shown in Fig. 4f, measurements using a 900-nm short-pass filter and a 1,000-nm short-pass filter indicate that light in the range  $900 \text{ nm} < \lambda < 1,600 \text{ nm}$  does not make a contribution to the PSV effect either. As for the situation shown in Fig. 4e, the data in Fig. 4f also show that the voltage (0.12 μV) measured with both the two filters used is very close to the value (0.11 μV) calculated using the multiplication rule, which further suggests that the critical wavelength is not in the range 900–1,600 nm. These results clearly suggest that the wavelength critical for the PSV effect lies in the range 1,600–2,000 nm.

In addition, the data obtained using the LED lamp and the 695-nm long-pass filter also confirm that the PSV effect is not

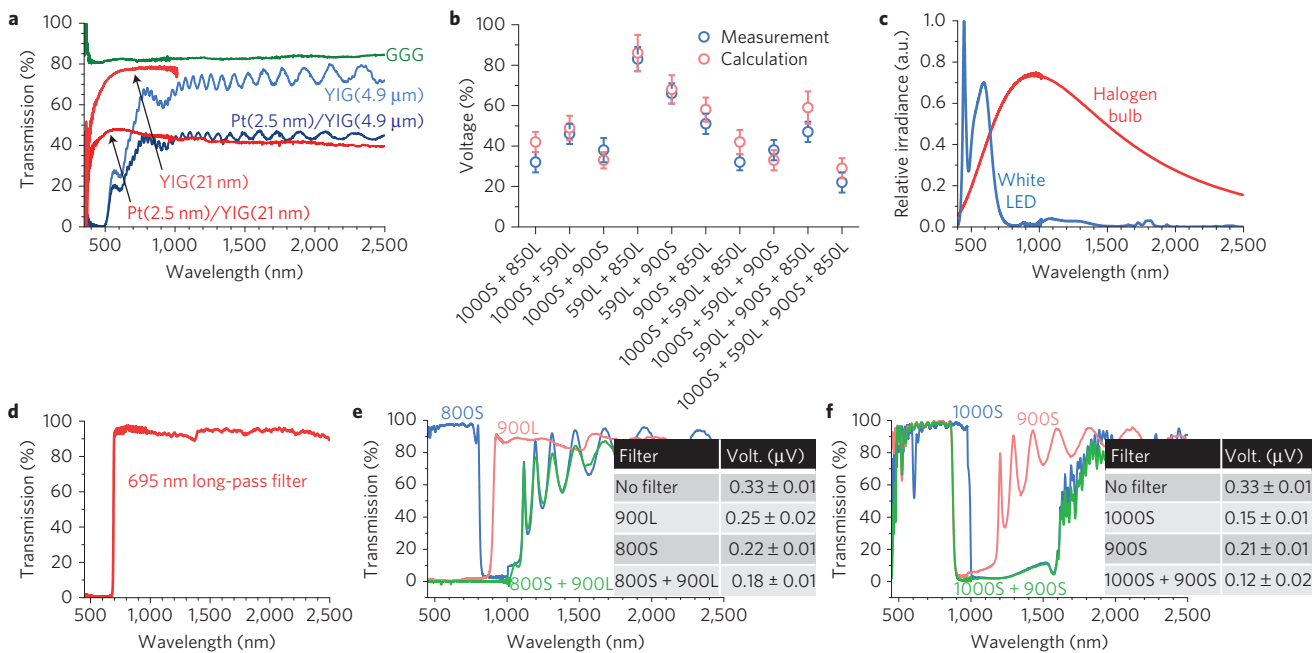


**Figure 4 | Measurements using different light sources and optical filters.** **a**, Optical transmission values of five samples. **b**, Voltages obtained using different filters (normalized to the voltage with no filter). The blue and red symbols show the measured and calculated voltages, respectively. ‘###S(L)’ denotes a ###-nm short-pass (long-pass) filter. The error bars are the standard deviations of the voltages measured during light illumination. **c**, Optical spectra of a 100-W halogen light bulb and a 40-W white LED lamp. **d**, Transmission profile of a long-pass filter. **e**, Optical transmission values of two filters used either separately or together. The table in **e** presents the measured voltages for the four filter configurations shown. **f**, Data of another two filters shown in the same format as in **e**.

associated with the excitations in the YIG. This statement is based on the facts that YIG films have a bandgap of about 2.8 eV (443 nm) and light with  $\lambda < 443$  nm can induce excitations in YIG films<sup>27</sup>. If the PSV effect relies on the excitations in the YIG, one would expect stronger voltage signals when the LED was used, because the LED emits a higher intensity of light in the range  $\lambda < 443$  nm than the halogen bulb, as shown in Fig. 4c; one would also anticipate no measurable signals when the 695-nm long-pass filter was used, because the filter shows no transmission in the  $\lambda < 695$  nm range.

On the basis of the experimental observations, it is believed that the PSV effect results from the photon-driven, spin-dependent excitation of electrons in Pt atoms that are in close proximity to the MI. More explicitly, this effect involves physical processes which are sketched in Fig. 5a and can be explained through density function theory (DFT) calculations for optical absorption<sup>28</sup> and spin diffusion analyses. Details on the calculations are provided in the Supplementary Information. The main microscopic processes are described below.

First, when light illuminates the Pt/MI structure, photons with an appropriate energy excite electrons in the occupied bands in the Pt to the unoccupied bands, as indicated by the left vertical arrow in the top diagram in Fig. 5a and the two vertical arrows in Fig. 5b.

Second, in paramagnetic Pt atomic layers, the light-induced excitation is expected to have the same efficiency for electrons in the two spin channels. However, the excitation is spin dependent for Pt atoms in close proximity to the MI (the gridded region in Pt in Fig. 5a), because those atoms are spin polarized and show ferromagnetic-like behaviour<sup>10,29–31</sup>. In other words, there are proximity-induced magnetic moments in the Pt atomic layers near the interface, and the presence of these moments gives rise to a difference in the excitation efficiency for electrons in the two spin channels. In fact, the DFT calculations indicate that the excitation of spin-down electrons is more efficient than that of spin-up electrons, as shown in Fig. 5c. The excitation process sketched in the top diagram in Fig. 5a is consistent with this result.

Third, the diffusion of the excited electrons and holes in the Pt from the ferromagnetic region to the paramagnetic region gives rise to spin currents  $J_e$  and  $J_h$ , respectively, as shown in the top diagram in Fig. 5a. At a first glance, there is no net spin flow because the electrons and holes carry exactly opposite spins. In practice, however, the holes in the occupied bands have lower energy, and thereby a longer spin mean free path than the electrons in the unoccupied bands. This difference results in a much larger spin current for the holes than for the electrons, and thus a net spin current  $J_{\text{net}} = J_e - J_h$ , as shown in Fig. 5d. The configuration shown in Fig. 5a corresponds to a net spin current that has a polarization along  $M$ , which is consistent with the spin flows depicted in Fig. 2a.

The above interpretation is qualitative in the sense that there is no clear boundary between the ferromagnetic and paramagnetic regions in the Pt. Nevertheless, the interpretation captures the essence of the physical process of the PSV effect and is supported by the experiments, as explained below.

First, because the PSV effect relies on the excitations in the Pt, not in the MI, one can expect similar voltage signals from samples made of different MIs. This expectation is met by the data shown in Fig. 3 which were obtained with four samples with very different MIs. One can also expect the absence of the PSV effect in samples where the Pt layer is replaced by other normal metals supporting no spin-dependent electron excitations. In fact, measurements using Cu/YIG and Cu/BaM yielded no notable PSV signals when  $\Delta T_1$  and  $\Delta T_1'$  were comparable to those cited above. When  $\Delta T_1$  was relatively large, we did observe voltage signals, which, however, changed with time in the same manner as  $\Delta T_1$ , as shown in Fig. 6a. These signals resulted from the Seebeck effect<sup>19</sup>.

Second, the sign of the spin voltage at the interface depends on the magnetic ordering in the Pt atomic layers in proximity to the MI, whereas the latter is induced by  $M$  in the MI<sup>29–31</sup>. For this reason, it is expected that a rotation of  $M$  in the MI will result in a change in the polarization of the spin current in the Pt, and the absence of the MI will give rise to no PSV signals. The first expectation is

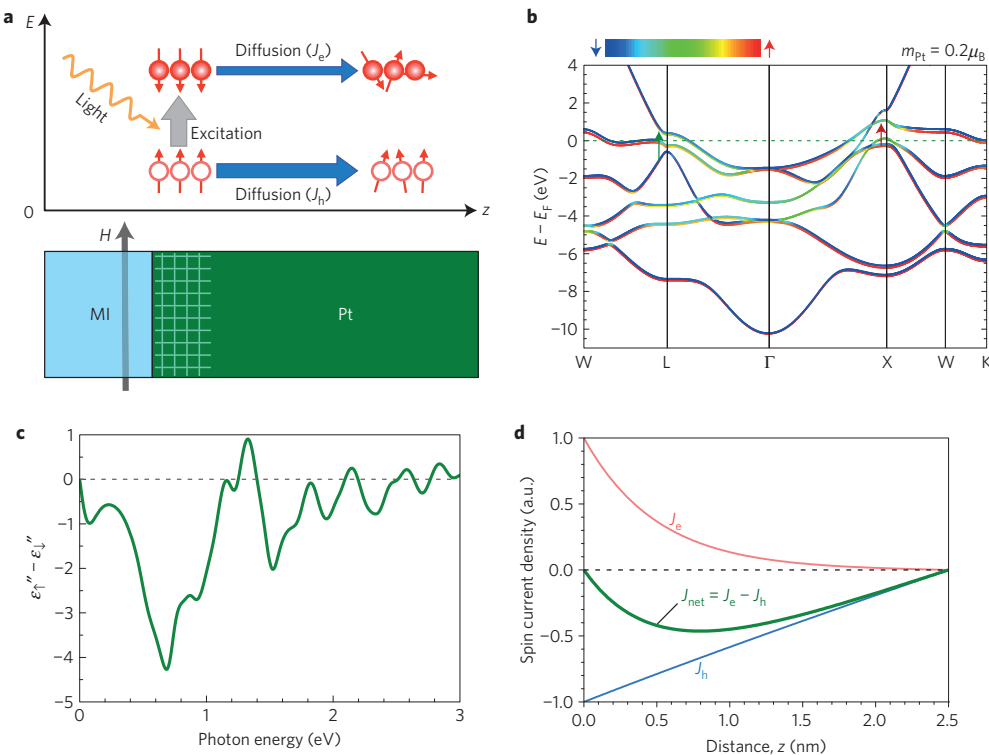


**Figure 5 | Theoretical interpretation.** **a**, Sketch of the physical mechanism underlying the PSV effect. When the light illuminates the sample, photons excite electrons and generate non-equilibrium hot electrons and holes in the Pt atomic layers that are in proximity to the MI (the gridded region). The excited electrons and holes diffuse from the Pt/MI interface to the Pt surface (along the  $+z$  direction), giving rise to spin currents ( $J_e$  and  $J_h$ ). **b**, Band structure of Pt calculated using DFT with spin-orbit coupling in the presence of a magnetic moment of  $0.2\mu_B$  per atom (where  $\mu_B$  is the Bohr magneton). **c**, Calculated difference between the imaginary parts of dielectric functions for the spin-up and spin-down channels. **d**, Spatial distributions of spin currents carried by hot electrons and holes. For the calculations, the Pt thickness was chosen to be 2.5 nm, and the spin mean free paths for the hot electrons and holes in the Pt film were chosen to be 0.5 nm and 5.0 nm, respectively.

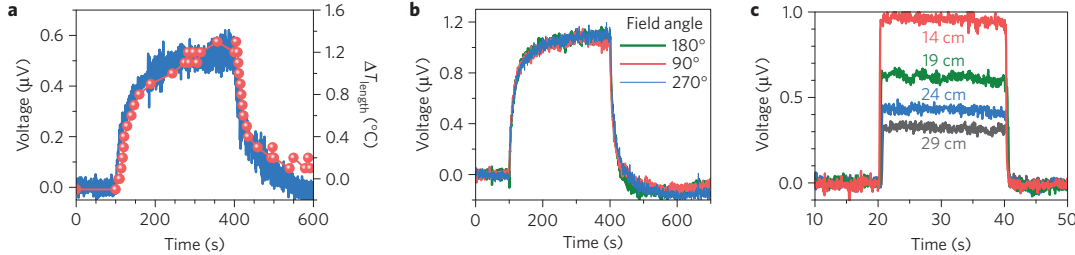


**Figure 6 | Control measurements.** **a**, Voltage (curve) and temperature (dots) signals measured across the length of a 20-mm-long, 1.75-mm-wide Cu(16 nm)/YIG(36  $\mu$ m)/GGG(0.4 mm) sample with **M** along the  $+y$  direction. **b**, Voltage signals obtained for three different field orientations from a 21-mm-long, 1.7-mm-wide Pt(8.5 nm)/GGG(0.5 mm) sample. **c**, Voltage responses for different light-to-sample distances obtained with a 18-mm-long, 1.65-mm-wide Pt(2.6 nm)/Ga-doped-YIG(78  $\mu$ m)/GGG(0.4 mm) sample with **M** along the  $+y$  direction. All the data were obtained using a 100-W halogen light bulb placed above the Cu or Pt side of the sample. For the data in **a,b**, the bulb was 10 cm away from the sample and was turned on at 100 s and off at 400 s. For the data in **c**, the bulb was turned on at 20 s and off at 40 s. The electrode separation was about 3.8 mm for all the measurements.

clearly shown by the dependence on the **M** orientation shown in Figs 2b and 3a,b. The second is proved by measurements on Pt/GGG samples. When  $\Delta T_1$  in Pt/GGG was relatively large, we observed only Seebeck-effect-produced voltage signals<sup>19</sup>, which changed with time in the same manner as  $\Delta T_1$ , and showed no dependence on the field direction, as shown in Fig. 6b.

Third, the excitation processes in the Pt should be independent of the direction of light illumination, which is consistent with the experimental observations for different light configurations shown in Figs 2c and 3a,b. This expectation is further confirmed by the data shown in Supplementary Fig. 4. The processes, however, depend on the light intensity, which is clearly indicated by the data in Fig. 6c as well as by the fact, shown in Fig. 3, that the voltage signal measured

for light illuminating both sides of a sample is equal to the sum of the signals for light illuminating one side of the sample.

Fourth, the theoretical results in Fig. 5c suggest that the PSV effect is strong in a relatively narrow wavelength region centred at about 0.7 eV. This agrees with the above-discussed experimental observations that the PSV effect depends only on a relatively narrow light wavelength range, and such wavelengths are most likely within the range 1,600–2,000 nm.

Last, besides the above-discussed qualitative agreements, there are also quantitative agreements between the experimental and theoretical results, as shown in Supplementary Fig. 1.

The PSV effect presented here differs from the phenomena of light-induced generation of spin currents reported previously<sup>32–43</sup>,

as explained below. First, the effects demonstrated in refs 32–38 occur in semiconductors only, not in normal metals. Furthermore, except for the case in ref. 38 they also require the use of polarized light. Second, the spin current generation presented in ref. 43 relies on the excitation of surface plasmon resonances. Finally, the effects reported in refs 39–42 made use of light to create a temperature gradient and the SSE to produce spin currents. In this case, the PSV effect and the SSE might coexist, as shown in Supplementary Fig. 4.

It is expected that the PSV effect should also occur in other normal metals that exhibit the magnetic proximity effect and strong spin-orbit coupling, including Pd<sup>44,45</sup>, W<sup>46</sup> and Ir<sup>46</sup>, as well as topological insulators<sup>47</sup>. Future work demonstrating the PSV effect in such materials would be of great interest. One can also expect that the PSV effect may open a door to new optical-spintronic applications, including light-based spin batteries, sensing orientations of magnetic moments or fields, and converting light energy to electricity.

Received 28 July 2015; accepted 22 March 2016;  
published online 25 April 2016

## References

- Urban, R., Woltersdorf, G. & Heinrich, B. Gilbert damping in single and multilayer ultrathin films: role of interfaces in nonlocal spin dynamics. *Phys. Rev. Lett.* **87**, 217204 (2001).
- Mizukami, S., Ando, Y. & Miyazaki, T. Effect of spin diffusion on Gilbert damping for a very thin permalloy layer in Cu/permalloy/Cu/Pt films. *Phys. Rev. B* **66**, 104413 (2002).
- Tserkovnyak, Y., Brataas, A. & Bauer, G. E. W. Enhanced Gilbert damping in thin ferromagnetic films. *Phys. Rev. Lett.* **88**, 117601 (2002).
- Uchida, K. *et al.* Observation of the spin Seebeck effect. *Nature* **455**, 778–781 (2008).
- Uchida, K. *et al.* Spin-Seebeck effects in Ni<sub>81</sub>Fe<sub>19</sub>/Pt films. *Solid State Commun.* **150**, 524–528 (2010).
- Jaworski, C. *et al.* Observation of the spin-Seebeck effect in a ferromagnetic semiconductor. *Nature Mater.* **9**, 898–903 (2010).
- Jaworski, C. *et al.* Spin-Seebeck effect: a phonon driven spin distribution. *Phys. Rev. Lett.* **106**, 186601 (2011).
- Jaworski, C., Myers, R., Johnston-Halperin, E. & Heremans, J. Giant spin Seebeck effect in a non-magnetic material. *Nature* **487**, 210–213 (2012).
- Uchida, K. *et al.* Spin Seebeck insulator. *Nature Mater.* **9**, 894–897 (2010).
- Qu, D., Huang, S. Y., Hu, J., Wu, R. & Chien, C. L. Intrinsic spin Seebeck effect in Au/YIG. *Phys. Rev. Lett.* **110**, 067206 (2013).
- Dyakonov, M. I. & Perel, V. I. Possibility of orienting electron spins with current. *JETP Lett.* **13**, 467–469 (1971).
- Hirsch, J. E. Spin Hall effect. *Phys. Rev. Lett.* **83**, 1834–1837 (1999).
- Day, C. Two groups observe the Spin Hall effect in semiconductors. *Phys. Today* **58**, 17–19 (February, 2005).
- Hoffmann, A. Spin Hall effects in metals. *IEEE Trans. Magn.* **49**, 5172–5193 (2013).
- Sun, Y. & Wu, M. in *Solid State Physics* Vol. 64 (eds Wu, M. & Hoffmann, A.) (Academic, 2013).
- Wu, M. in *Advanced Magnetic Materials* (ed. Malkinski, L.) (InTech, 2012).
- Valenzuela, S. O. & Tinkham, M. Direct electronic measurement of the spin Hall effect. *Nature* **442**, 176–179 (2006).
- Kittel, C. *Introduction to Solid State Physics* 8th edn (John Wiley, 2005).
- DiSalvo, F. J. Thermoelectric cooling and power generation. *Science* **285**, 703–706 (1999).
- Huebener, R. P. & Seher, A. Nernst effect and flux flow in superconductors. I. Niobium. *Phys. Rev.* **181**, 701–709 (1969).
- Pu, Y., Johnston-Halperin, E., Awschalom, D. D. & Shi, J. Anisotropic thermopower and planar Nernst effect in Ga<sub>1-x</sub>Mn<sub>x</sub>As ferromagnetic semiconductors. *Phys. Rev. Lett.* **97**, 036601 (2006).
- Huang, S. Y., Wang, W. G., Lee, S. F., Kwo, J. & Chien, C. L. Intrinsic spin-dependent thermal transport. *Phys. Rev. Lett.* **107**, 216604 (2011).
- Ky, V. D. The planar Nernst effect in permalloy films. *Phys. Status Solidi B* **17**, K207–K209 (1966).
- Avery, A. D., Pufall, M. R. & Zink, B. L. Observation of the planar Nernst effect in permalloy and nickel thin films with in-plane thermal gradients. *Phys. Rev. Lett.* **109**, 196602 (2012).
- Yin, S. L., Mao, Q., Meng, Q. Y., Li, D. & Zhao, H. W. Hybrid anomalous and planar Nernst effect in permalloy thin films. *Phys. Rev. B* **88**, 064410 (2013).
- Kehlberger, A. *et al.* Length scale of the spin Seebeck effect. *Phys. Rev. Lett.* **115**, 096602 (2015).
- Jakubisova-Liskova, E., Visnovsky, S., Chang, H. & Wu, M. Optical spectroscopy of sputtered nanometer-thick yttrium iron garnet films. *J. Appl. Phys.* **117**, 17B702 (2015).
- Hughes, J. L. P. & Sipe, J. E. Calculation of second-order optical response in semiconductors. *Phys. Rev. B* **53**, 10751–10763 (1996).
- Huang, S. Y. *et al.* Transport magnetic proximity effects in platinum. *Phys. Rev. Lett.* **109**, 107204 (2012).
- Lu, Y. M. *et al.* Pt magnetic polarization on Y<sub>3</sub>Fe<sub>5</sub>O<sub>12</sub> and magnetotransport characteristics. *Phys. Rev. Lett.* **110**, 147207 (2013).
- Zhou, X. *et al.* Tuning magnetotransport in PdPt/Y<sub>3</sub>Fe<sub>5</sub>O<sub>12</sub>: effects of magnetic proximity and spin-orbit coupling. *Appl. Phys. Lett.* **105**, 012408 (2014).
- Ganichev, S. D. *et al.* Spin-galvanic effect. *Nature* **417**, 153–156 (2002).
- Leyder, C. *et al.* Observation of the optical spin Hall effect. *Nature Phys.* **3**, 628–631 (2007).
- Miah, M. Observation of the anomalous Hall effect in GaAs. *J. Phys. D* **40**, 1659–1669 (2007).
- Wunderlich, J. *et al.* Spin Hall effect transistor. *Science* **330**, 1801–1804 (2010).
- Ando, K. *et al.* Direct conversion of light-polarization information into electric voltage using photoinduced inverse spin-Hall effect in Pt/GaAs hybrid structure: spin photodetector. *J. Appl. Phys.* **107**, 113902 (2010).
- Kampfrath, T. *et al.* Terahertz spin current pulses controlled by magnetic heterostructures. *Nature Nanotech.* **8**, 256–260 (2013).
- Endres, B. *et al.* Demonstration of the spin solar cell and spin photodiode effect. *Nature Commun.* **4**, 2068 (2013).
- Weiler, M. *et al.* Local charge and spin currents in magnetothermal landscapes. *Phys. Rev. Lett.* **108**, 106602 (2012).
- Agrawal, M. *et al.* Role of bulk-magnon transport in the temporal evolution of the longitudinal spin-Seebeck effect. *Phys. Rev. B* **89**, 224414 (2014).
- Li, P. *et al.* Generation of pure spin currents via spin Seebeck effect in self-biased hexagonal ferrite thin films. *Appl. Phys. Lett.* **105**, 242412 (2014).
- Roschewsky, N. *et al.* Time resolved spin Seebeck effect experiments. *Appl. Phys. Lett.* **104**, 202410 (2014).
- Uchida, K. *et al.* Generation of spin currents by surface plasmon resonance. *Nature Commun.* **6**, 5910 (2015).
- Fullerton, E. E. *et al.* Structure and magnetism of epitaxially strained Pd(001) films on Fe(001): experiment and theory. *Phys. Rev. B* **51**, 6364–6378 (1995).
- Bailey, W. E. *et al.* Pd magnetism induced by indirect interlayer exchange coupling. *Phys. Rev. B* **86**, 144403 (2012).
- Wilhelm, F. *et al.* Systematics of the induced magnetic moments in 5d layers and the violation of the third Hund's rule. *Phys. Rev. Lett.* **87**, 207202 (2001).
- Lang, M. *et al.* Proximity induced high-temperature magnetic order in topological insulator - ferrimagnetic insulator heterostructure. *Nano Lett.* **14**, 3459–3465 (2014).

## Acknowledgements

This work was primarily supported by the US Army Research Office under Award W911NF-14-1-0501. In addition, the fabrication and structural characterization of YIG, YIG/Pt, YIG/Cu and GGG/Pt samples and the DFT calculations were supported by the SHINES, an Energy Frontier Research Center funded by the US Department of Energy, Office of Science, Basic Energy Sciences under Award SC0012670; the fabrication and structural characterization of BaM, BaM/Pt and BaM/Cu samples was supported by the C-SPIN, one of the SRC STARnet Centers sponsored by MARCO and DARPA; and the ferromagnetic resonance and spin pumping measurements were supported by the US National Science Foundation under Award ECCS-1231598. The authors would like to thank J. Sites and J. Raguse of the CSU Photovoltaics Laboratory for helpful discussions regarding optical spectroscopy.

## Author contributions

L.L., D.E. and M.W. conceived the idea and designed the experiments. L.L. established the experimental set-up. D.E. and L.L. performed the measurements and analysed the data. H.C. and P.L. fabricated and characterized the samples. B.J. contributed to the experimental set-up. Y.B. contributed to the measurements. J.L., J.X. and R.W. provided the theoretical model. J.L., Z.W. and J.H. performed the calculations. M.W. supervised the experimental study. R.W. supervised the theoretical study. D.E., J.L., R.W. and M.W. wrote the paper and the Supplementary Information with help from all the other co-authors.

## Additional information

Supplementary information is available in the online version of the paper. Reprints and permissions information is available online at [www.nature.com/reprints](http://www.nature.com/reprints).

Correspondence and requests for materials should be addressed to R.W. or M.W.

## Competing financial interests

The authors declare no competing financial interests.